Journal of Power Sources 233 (2013) 299–303

Contents lists available at SciVerse ScienceDirect

Journal of Power Sources

journal homepage: www.elsevier.com/locate/jpowsour

Short communication

# A hybrid phase-transition model of olivine $LiFePO_4$ for the charge and discharge processes

De Li [a], Tao Zhang [a], Xizheng Liu [a], Ping He [b], Ruwen Peng [b], Mu Wang [b], Min Han [b], Haoshen Zhou [a,b,*]

[a] Energy Technology Research Institute, National Institute of Advanced Industrial Science and Technology (AIST), Umezono, 1-1-1, Tsukuba 305-8568, Japan
[b] National Laboratory of Solid State Microstructures & Department of Energy Science and Engineering, Nanjing University, Nanjing 210093, China

## HIGHLIGHTS

- The Warburg impedance is dependent on the phase and the applied potential.
- The domino-cascade model leads to a tilt angle of 30° in the Warburg region.
- A hybrid phase-transition model of domino-cascade model and core–shell model.
- This hybrid model is due to the strong anisotropy and the two-phase difference.

## ARTICLE INFO

*Article history:*
Received 5 November 2012
Received in revised form
27 December 2012
Accepted 19 January 2013
Available online 28 January 2013

*Keywords:*
Lithium-ion battery
$LiFePO_4$
Electrochemical impedance spectroscopy (EIS)
Domino-cascade model
Core–shell model

## ABSTRACT

Generally, it is well known that the lithium-ion diffusion in olivine $Li_xFePO_4$ is correlated with the phase transition dominated by a domino-cascade model instead of a core–shell model. Based on the experiment result, we firstly found that the linear Warburg region of electrochemical impedance spectra should tilt with a small angle of 30° for the domino-cascade model, while the core–shell model should correspond to a traditional angle of about 45°. Considering that the measured Warburg impedance varies along the charge and discharge processes, we firstly proposed a hybrid phase-transition model as a combination of the domino-cascade model and the core–shell model to describe the olivine $Li_xFePO_4$. And this hybrid model was possibly attributed to both the strong anisotropy in the bulk of olivine $Li_xFePO_4$ and the different properties between the lithiated and delithiated phases. Potentially, this micro-mechanism could be extended to some other two-phase electrode active materials in lithium ion batteries.



## 1. Introduction

Following the pioneering work of Padhi et al. in 1997 [1], a lot of effort has been made to the development the olivine $LiFePO_4$ as a cathode material in lithium ion batteries [2]. As the olivine $LiFePO_4$ is poor at electronic and ionic conductivities, its electrochemical performances are usually improved through carbon coating [3], cation doping [4], off-stoichiometry and so on. Besides, for the lithium-ion diffusion is very slow especially companying with the phase transition, the nanoscale particles are usually adopted to reduce the diffusion length [5]. Meanwhile, plenty of works have been contributed to figure out the micro-mechanism of the phase transition in olivine $Li_xFePO_4$. It is well known that the olivine $Li_xFePO_4$ is a two-phase structure at room temperature [6,7], where both the lithiated (beta) and delithiated (alpha) phases are of the same crystal structure, as shown in Fig. 1. In this structure, the corner-sharing $FeO_6$ octahedra form a distorted two-dimensional square lattice perpendicular to the *a*-axis and the tetrahedral $PO_4$ groups connect neighboring planes, so that the lithium ions migrate in the parallel chains along the *b*-axis [8]. Currently, it is well accepted that the phase transition follows the domino-cascade model [9] during the (dis)charge process, where the lithium ions (de)intercalate into $Li_xFePO_4$ through the two-phase boundary in the *bc*-plane and the boundary moves along the *a*-axis. However, the nanoscale particles, the big current or potential step will suppress the phase separation and the system will bypass nucleation and growth of a second phase through a single-phase transformation path [10–13], which makes the phase transformation more complex in olivine $Li_xFePO_4$ [14].

* Corresponding author. Energy Technology Research Institute, National Institute of Advanced Industrial Science and Technology (AIST), Umezono, 1-1-1, Tsukuba 305-8568, Japan. Tel.: +81 29 861 5795; fax: +81 29 861 3489.
*E-mail address:* hs.zhou@aist.go.jp (H. Zhou).

0378-7753/$ – see front matter © 2013 Elsevier B.V. All rights reserved.
http://dx.doi.org/10.1016/j.jpowsour.2013.01.133

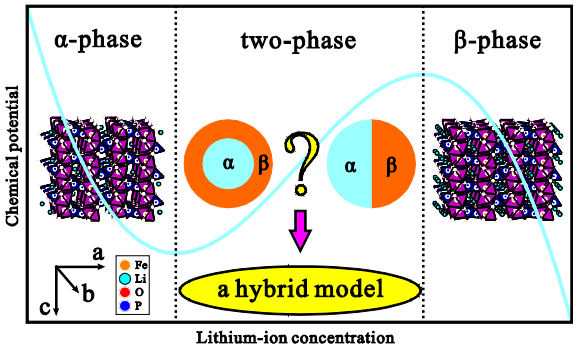


**Fig. 1.** The crystal structures of olivine $Li_xFePO_4$ for the single alpha and beta phases, and a hybrid phase-transition model is proposed to challenge the domino-cascade model and the core–shell model in the two-phase region. Here, the cyan curve represents the chemical potential profile of the olivine $Li_xFePO_4$. (For interpretation of the references to color in this figure legend, the reader is referred to the web version of this article.)

In this work, we investigated the lithium-ion diffusion and phase transition in olivine $LiFePO_4$ with a mean particle size of 3 μm, using Electrochemical Impedance Spectroscopy (EIS) [15,16] where the Warburg region in the low frequency is dominated by the lithium-ion diffusion. In the EIS spectra, a small tilt angle of 30° was observed in the linear Warburg region, and it was reported that the small tilt angle was attributed to the movement of the two-phase boundary [17]. Accurately, the tilt angle of 30° was due to that the lithium-ion diffusion could couple with the movement of two-phase boundary in the domino-cascade model. When trying to confirm the domino-cascade model in the olivine $Li_xFePO_4$ by the EIS spectra, we found that the phase transition can not be simply described by the current domino-cascade model or the previous core–shell model, as shown in Fig. 1. Instead, a hybrid phase-transition model [18] was proposed as the combination of the domino-cascade model and the core–shell model.

## 2. Experiments

The commercial $LiFePO_4$ (SLFP-PD60) was purchased from Tianjin STL Energy Technology Co., Ltd., China. As the SEM image shown in Fig. 2(a), the SLFP-PD60 is an assemble of the primary $LiFePO_4$ particles with a mean size of ~3 μm, and about 2 wt.% of carbon is contained to improve the electronic conductivity. Obviously, all the particles are not identical for the size, the shape and the position, so the electrochemical measurements would give a statistical result for this sample. In the working electrode, as shown in Fig. 2(b), the SLFP-PD60 paste with a thickness of ~30 μm is pressed on an aluminum mesh (100 mesh) with a diameter of ~10 mm and a mass loading of ~5 mg $cm^{-2}$, where the paste contains 80 wt.% SLFP-PD60, 15 wt.% acetylene black and 5 wt.% polytetrafluoroethylene (PTFE). Lithium metal was used as both counter and reference electrodes on copper meshes (100 mesh). And the electrolyte was 1 M $LiClO_4$ in ethylene carbonate/diethyl carbonate (EC/DEC with volume ratio of 1:1). A three-electrode glass cell was used in the electrochemical measurements, and the cell assembly was carried out in a glovebox in an argon atmosphere. The charge–discharge test and the EIS measurement were carried out using both a Solartron Analytical 1287 Electrochemical interface with a model 1255b Impedance Analyzer and an Autolab electrochemical instrument with a FRA2 frequency response analyser.

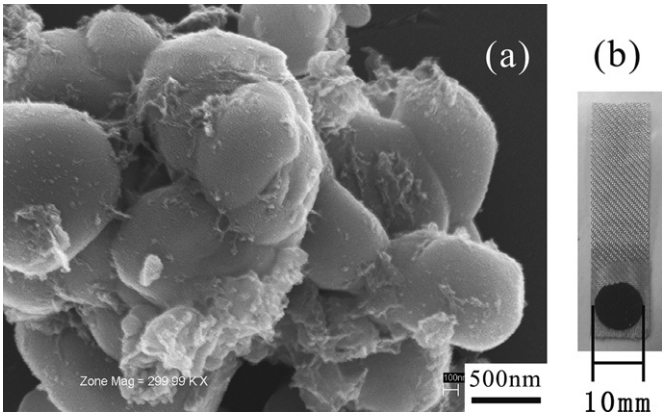


**Fig. 2.** (a) The SEM image of the commercial $LiFePO_4$ (SLFP-PD60). (b) As the working electrode, the SLFP-PD60 paste with a thickness of ~30 μm is pressed on an aluminum mesh with a diameter of ~10 mm and a mass loading of ~5 mg $cm^{-2}$.

## 3. Results and discussion

Firstly, two single phases are studied to obtain their electrochemical properties separately. In the measurement, the glass cell keeps potentiostatic for 10 min, and then EIS measurement is carried out at that potential, where the amplitude of the applied AC signal is 5 mV and each EIS measurement takes about 10 min. In the beta phase (discharged state), nine potentials from 3.385 V to 3.465 V were applied on the electrode and the active material was gradually charged into the two-phase region by increasing the potential, as shown in the right of Fig. 3(a), where the short flat lines indicate the potentiostatic processes and the curve connect the end of each potential after the EIS measurement. After charging at the current of 0.1 C, the olivine $Li_xFePO_4$ was converted into the alpha phase. Then, nine potentials from 3.465 V to 3.385 V were applied on the alpha phase and the active material was discharged into the two-phase region, as shown in the left of Fig. 3(a).

In order to obtain the chemical potential profile for both phases, we need to remove the potential component that drives the current. Thus, the curve of potential vs. offset DC current in EIS measurements ($E$ vs. $I$) is plotted in the right and left of Fig. 3(b), for the beta and alpha phases, respectively. When the potential is higher than 3.445 V for beta phase and lower than 3.415 V for the alpha phase, the current was decreased to several μA in 10 min. Otherwise, the current will tend to a constant value and the state of electrode will evidently change with time, so each potential only takes 10 min to make the working electrode stable for EIS measurement. For the beta phase, the current linearly increases with the potential when the potential gets across a threshold value of about 3.447 V, and the corresponding resistance is 158 Ω for the DC current. Meanwhile, the threshold potential is about 3.413 V and the resistance is 194 Ω for the alpha phase. Then, the potential component on the resistance was removed from the applied potential, so that the $E$ vs. $x$ ($x$ in $Li_xFePO_4$) curve in Fig. 3(a) is modified into the chemical potential profile in the middle of Fig. 3(b). In the chemical potential profile, the spinodal points are corresponding to the highest potential for the beta phase and the lowest potential for the alpha phase, respectively, which correspond to the knee points in the $E$ vs. $I$ curves. And the black dashed curve connecting two spinodal points indicates a single-phase transformation path. As the applied potential is beyond the spinodal point for each phase, the phase separation would take place through spinodal decomposition, and the two-phase transformation paths would be the flat dashed arrows for the charge and discharge processes, respectively.

The EIS spectra measured from $10^4$ Hz to $10^{-2}$ Hz are plotted in Fig. 4(a) and (b) for the alpha and beta phases, respectively, where each Nyquist plot possesses a high-frequency depressed semicircle and a linear Warburg region below the frequency of 5 Hz. Actually,

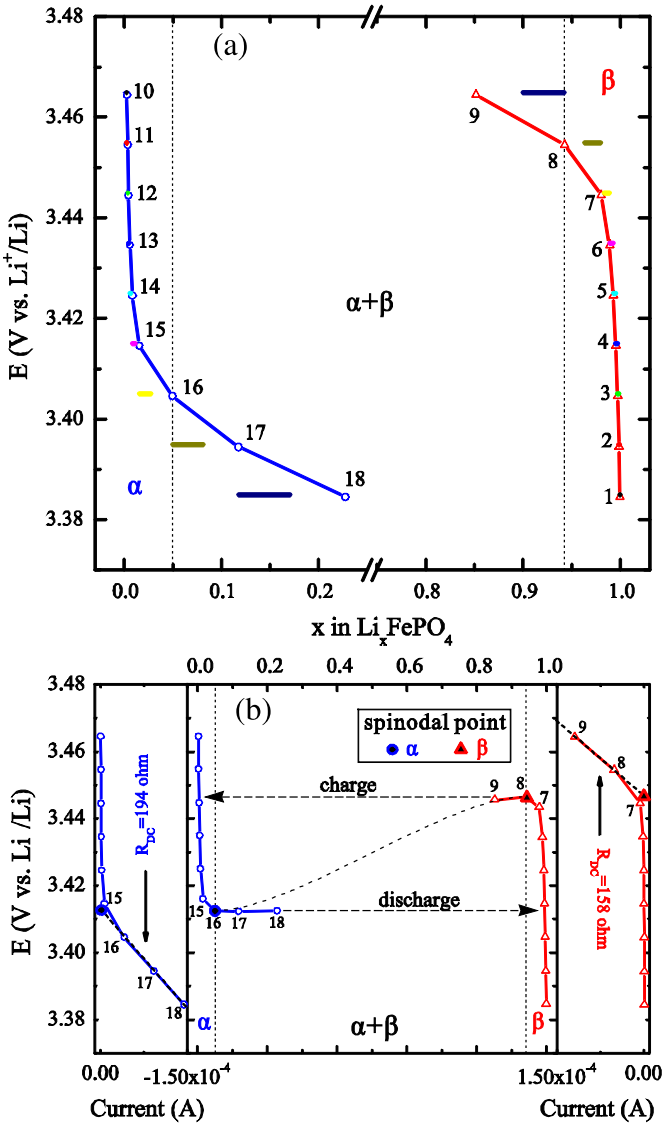


**Fig. 3.** (a) Nine potentiostatic charging from 3.385 V to 3.465 V for the beta phase and nine potentiostatic discharging from 3.465 V to 3.385 V for the alpha phase before each corresponding EIS measurement, where the short flat lines indicate the potentiostatic processes and the curve connect the end of each potential after the EIS measurement. (b) The chemical potential profile of $Li_xFePO_4$ in a single-phase transformation path, and the curve of potential vs. current (the offset DC current in EIS measurements) for the alpha (beta) phase in the left (right).

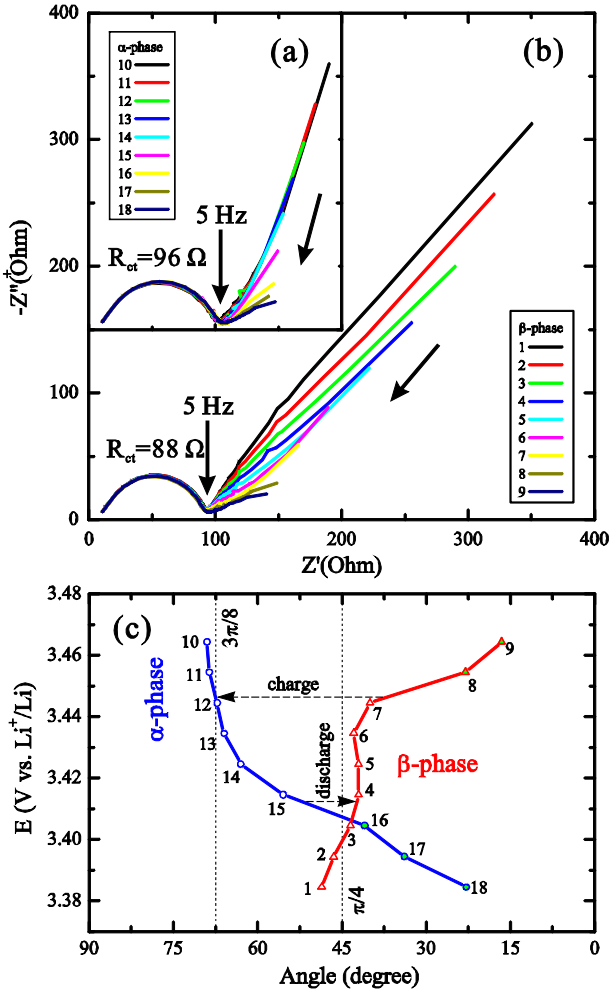


**Fig. 4.** The EIS spectra from $10^4$ Hz to $10^{-2}$ Hz measured at different potentials for the (a) alpha and (b) beta phase. (c) The tilt angle in the linear Warburg region of EIS spectra for the alpha and beta phase, as the blue and red curves respectively. (For interpretation of the references to color in this figure legend, the reader is referred to the web version of this article.)

this semicircle originates from the parallel connection of a charge-transfer resistance ($R_{ct}$) related to lithium-ion interfacial transfer and a double-layer capacitance at the electrolyte/electrode interface. Here, the $R_{ct}$ is evaluated as the diameter, which is about 96 Ω for the alpha phase and 88 Ω for the beta phase. In the Warburg region, the amplitude of impedance becomes smaller when the applied potential approaches the spinodal point for both the charge and discharge processes. Meanwhile, the tilt angle of Warburg impedance is about 67.5° for the alpha phase above the potential of 3.435 V and it linearly decreases to 23° at the potential of 3.385 V, as the blue curve in Fig. 4(c). In contrast, the tilt angle is about 45° for the beta phase and it drops down to 17° when the potential gets across the spinodal point, as the red curve in Fig. 4(c). Usually, the tilt angle in the Warburg region is 45° for a single phase, and it is less than 45° in the two-phase region due to the movement of two-phase boundary, such as Points 8, 9, 16, 17 and 18.

Secondly, the EIS spectra in the two-phase region were measured point by point during the (dis)charging process at the current of 0.1 C, as shown in Fig. 5(a). In the (dis)charge process, the cell was switched off every 1 h and kept open circuit for 1 h before the EIS measurement. And the EIS spectra were measured from $10^4$ Hz to $10^{-2}$ Hz at Open Circuit Potential (OCP), which are presented as Nyquist plots in Fig. 5(b) and (c) for the charge and discharge processes, respectively. For this cell, the high-frequency depressed semicircle and a linear Warburg region is separated at the frequency of 40 Hz. The $R_{ct}$ for the charge process varies from 20 Ω to 24 Ω, and it only increases from 25 Ω to 27 Ω for the discharge process.

The linear Warburg region is contributed by lithium-ion diffusion inside $Li_xFePO_4$ particles and the diffusion coefficient ($D_{Li}$) can be derived from the expression as

$$D_{Li} = \frac{1}{2}\left[\left(\frac{V_m}{FA\sigma_w}\right)\frac{dE}{dx}\right]^2 \quad (1)$$

where $V_m$ is the molar volume of $LiFePO_4$ (43.82 $cm^3\ mol^{-1}$), $F$ is the Faraday constant, $A$ is the total contact area between the electrolyte and the electrode, $dE/dx$ should be the slope of (dis)charge curve,

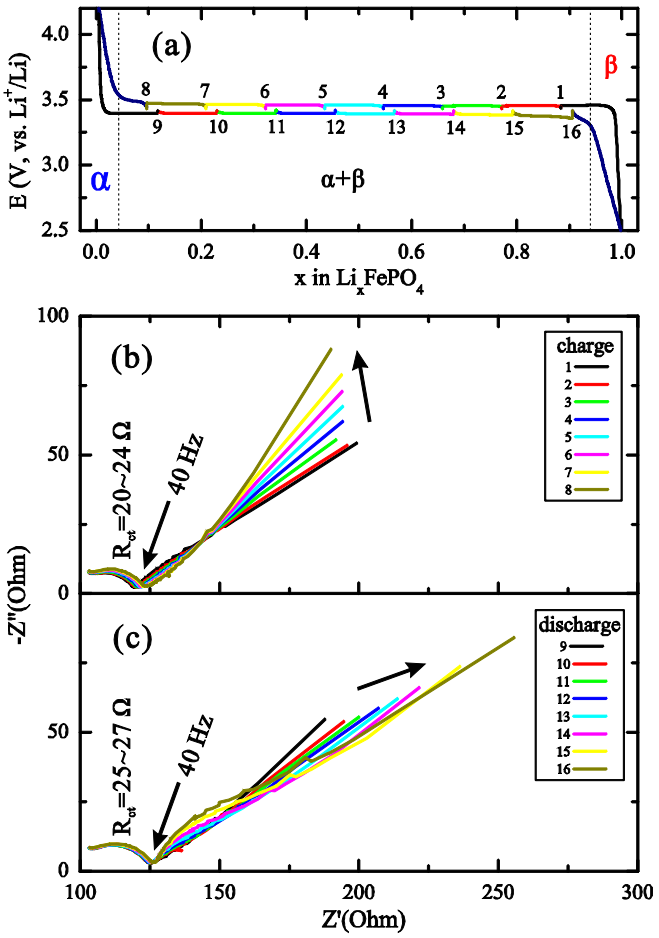


**Fig. 5.** (a) The charge–discharge curve at the current of 0.1 C, where the cell is switched off every 1 h for EIS measurement with one-hour relaxation. The EIS spectra from $10^4$ Hz to $10^{-2}$ Hz measured at different states of (b) charge and (c) discharge in the two-phase region. Here, a resistance of 100 Ω is in series connected with the glass cell to prevent from the big current during EIS measurement.

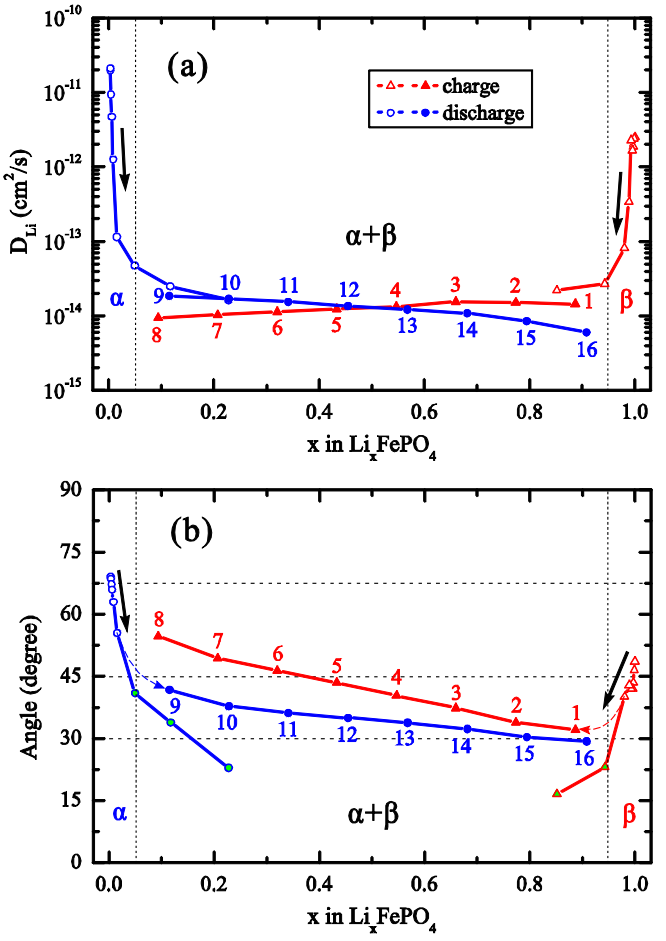


**Fig. 6.** (a) The lithium-ion diffusion coefficient as a function of $x$ in $Li_xFePO_4$, and (b) the tilt angle in the linear Warburg region of EIS spectra.

and the Warburg coefficient $\sigma_w$ is the fitted slope of $Z'$ vs. $\omega^{1/2}$ plot in the Warburg region of EIS spectra, where $\omega$ is the angular frequency. In the single phases, the d$E$/d$x$ is taken from the (dis)charge curve in Fig. 3(a) and the $\sigma_w$ is extracted from the EIS spectra in Fig. 4(a) and (b).

Actually, Eq. (1) was originally derived for the single-phase electrode. For the two-phase system, it is not a real diffusion coefficient of lithium-ion diffusion, but an apparent coefficient which is determined by the diffusion in the single phases and along or across the two-phase boundary. Usually, the lithium-ion diffusion is limited by the two-phase boundaries inside the particles, so the apparent coefficient should be smaller than that in the single phase. In the two-phase region, the (dis)charge curve is nearly a flat plateau without potential gradient, as shown in Fig. 5(a), and the d$E$/d$x$ in the Eq. (1) should be evaluated by the contribution of both phases and their boundary. Considering it is still unclear about the two-phase configuration inside the $LiFePO_4$ particles, the d$E$/d$x$ is set as the average value between the spinodal point of two phases, as Point 8 and Point 16 in Fig. 3(a). Besides, the $\sigma_w$ is extracted from the EIS spectra in Fig. 5(b) and (c) for the two-phase region. According to Eq. (1), the $D_{Li}$ is plotted as a function of lithium concentration ($x$ in $Li_xFePO_4$) in Fig. 6(a), where the red and blue curves (in the web version) are corresponding to the charge and discharge processes, respectively. In the two-phase region, both the $D_{Li}$ in the charge and discharge processes are in the magnitude of $10^{-14}$ cm$^2$ s$^{-1}$, which are smaller than those for the single phases as we expected.

Meanwhile, the tilt angle in the Warburg region varies during the (dis)charge process, as shown in Fig. 5(b) and (c). In the two-phase region, it increases from 32° to 55° in the charge process, while it decrease from 42° to 29° in the discharge process, as the red and blue curves (in the web version) in Fig. 6(b), respectively. In comparison, the tilt angle is about 67.5° for the alpha phase and it is about 45° for the beta phase. As shown in Fig. 4(c), when the charge and discharge processes follow the dashed arrows, the tilt angle should vary from 36.5° to 67.5° in the charge process and from 52° to 42.5° in the discharge process, which is different from the measured result. Thereby, the EIS spectra are not contributed by the alpha phase and beta phase separately, but two phases should be arranged in a special configuration and the two-phase boundary plays an important role in the EIS spectra. In olivine $Li_xFePO_4$ with strong anisotropy, the phase transition is usually described with the domino-cascade model for the (dis) charge process, so that the lithium-ion diffusion in both phases is coupled with the movement of the two-phase boundary. Previously, there are ever some reports about the tilt angle in the Warburg region that is less than 45° and close to 30° for two-phase active materials in lithium ion batteries [17], and this property was normally attributed to the slow movement of two-phase boundary. Thus, the small tilt angle of about 30° should be attributed to the domino-cascade model here. Besides, the tilt angle is not always 30° in the measured EIS spectra and it is unsymmetrical between

the charge and discharge processes, possibly due to the different properties between the alpha and beta phases.

In the experiment, the olivine $LiFePO_4$ (SLFP-PD60) possesses a mean particle size of 3 μm, so that the lithium ions will diffuse inside the particles slowly. As a result, two phases will coexist inside a single particle in the two-phase region. As we attributed the small tilt angle of about 30° to the domino-cascade model, the tilt angle up to 55° in the charge process should result from another two-phase model [19]. In this case, the two-phase boundary should not connect with the particle surface, and the lithium ions will insert into or extract from a single phase outside, which corresponds to the core–shell model. Actually, these two simple models are very popular in two-phase active materials and more complex configurations are rarely reported in such micro-particles. Thereby, we proposed a hybrid phase-transition model that was the combination of the domino-cascade model and the core–shell model, according to the tilt angle in Fig. 6(b). For the charge process, the lithium ions are extracted from the single beta phase and the tilt angle is about 45°. By charging, the alpha phase emerges on the surface and it grows up in the domino-cascade model, so that the tilt angle is 32°. Then, the alpha phase gradually occupies the surface of the particle and the tilt angle becomes bigger. As the whole surface is converted into the alpha phase, the phase transition is controlled by the core–shell model, which conflicts with some reports that the beta phase prefers outside of the particles for the volume expansion [20]. Since the single alpha phase corresponds to a tilt angle of 67.5°, the tilt angle gradually approaches the value during the charge process. In the end, the beta core in the center will vanish and the particle becomes the single alpha phase. In the beginning of discharging, the tilt angle is 67.5° for the single alpha phase under a high potential, and it drops down to 42° as the particle gets into the two phase region. In this period, the beta phase grows up by some nuclei on the surface, and the lithium ions mainly insert into the particle through the alpha phase. As the two-phase boundary is established gradually, the lithium ions prefer inserting through the two-phase boundary in the domino-cascade model. Gradually, the tilt angle decreases to 29° and the system is completely controlled by the domino-cascade model. In the end, the particles are converted into the single beta phase with a tilt angle of about 45°.

## 4. Conclusions

In this work, we investigated the lithium-ion diffusion and phase transition in olivine $Li_xFePO_4$ by EIS spectra, of which the Warburg region was determined by the lithium-ion diffusion. We firstly found that the linear Warburg region of EIS spectra should tilt with a small angle of 30° when the phase transition was dominated by the domino-cascade model, while the core–shell model should correspond to a traditional angle of about 45°. Actually, the lithium-ion diffusion would couple with the movement of two-phase boundary in the domino-cascade model. Considering that the measured Warburg impedance varies along the charge and discharge processes, we proposed a hybrid phase-transition model to describe olivine $Li_xFePO_4$, which was possibly attributed to both the strong anisotropy in the bulk of olivine $Li_xFePO_4$ and the different properties between two phases. In this hybrid model, the $Li_xFePO_4$ particle starts with the domino-cascade model and it is soon controlled by the core–shell model during the charge process. During the discharge process, the beta nuclei are formed on the surface and then the $Li_xFePO_4$ particle is quickly dominated by the domino-cascade model. Potentially, this micro-mechanism could be extended to some other two-phase electrode active materials in lithium ion batteries.

## References

[1] A.K. Padhi, K.S. Nanjundaswamy, J.B. Goodenough, J. Electrochem Soc. 144 (1997) 1188–1194.
[2] B. Kang, G. Ceder, Nature 458 (2009) 190–193.
[3] Y.G. Wang, Y.R. Wang, E.J. Hosono, K.X. Wang, H.S. Zhou, Angew. Chem. Int. Ed. 47 (2008) 7461–7465.
[4] S.Y. Chung, J.T. Bloking, Y.M. Chiang, Nat. Mater. 1 (2002) 123–128.
[5] R. Malik, D. Burch, M. Bazant, G. Ceder, Nano Lett. 10 (2010) 4123–4127.
[6] A. Yamada, H. Koizumi, S.I. Nishimura, N. Sonoyama, R. Kanno, M. Yonemura, T. Nakamura, Y. Kobayashi, Nat. Mater. 5 (2006) 357–360.
[7] C. Delacourt, P. Poizot, J.M. Tarascon, C. Masquelier, Nat. Mater. 4 (2005) 254–260.
[8] S. Nishimura, G. Kobayashi, K. Ohoyama, R. Kanno, M. Yashima, A. Yamada, Nat. Mater. 7 (2008) 707–711.
[9] C. Delmas, M. Maccario, L. Croguennec, F. Le Cras, F. Weill, Nat. Mater. 7 (2008) 665–671.
[10] P. Gibot, M. Casas-Cabanas, L. Laffont, S. Levasseur, P. Carlach, S. Hamelet, J.M. Tarascon, C. Masquelier, Nat. Mater. 7 (2008) 741–747.
[11] R. Malik, F. Zhou, G. Ceder, Nat. Mater. 10 (2011) 587–590.
[12] P. Bai, D.A. Cogswell, M.Z. Bazant, Nano Lett. 11 (2011) 4890–4896.
[13] G. Oyama, Y. Yamada, R. Natsui, S. Nishimura, A. Yamada, J. Phys. Chem. C 116 (2012) 7306–7311.
[14] N. Sharma, X.W. Guo, G.D. Du, Z.P. Guo, J.Z. Wang, Z.X. Wang, V.K. Peterson, J. Am. Chem. Soc. 134 (2012) 7867–7873.
[15] K. Tang, X.Q. Yu, J.P. Sun, H. Li, X.J. Huang, Electrochim. Acta 56 (2011) 4869–4875.
[16] A.K. Hjelm, G. Lindbergh, Electrochim. Acta 47 (2002) 1747–1759.
[17] S.I. Pyun, J.S. Bae, Electrochim. Acta 41 (1996) 919–925.
[18] D. Li, P. He, H.Q. Li, H.S. Zhou, Phys. Chem. Chem. Phys. 14 (2012) 9086–9091.
[19] D. Li, Z. T., X.Z. Liu, P. He, R.W. Peng, M. Wang, M. Han, H.S. Zhou, J. Power Sources, submitted for publication.
[20] L. Laffont, C. Delacourt, P. Gibot, M.Y. Wu, P. Kooyman, C. Masquelier, J.M. Tarascon, Chem. Mater. 18 (2006) 5520–5529.